Arab J Sci Eng (2014) 39:8157–8174
DOI 10.1007/s13369-014-1310-5

RESEARCH ARTICLE - MECHANICAL ENGINEERING

Free Convection Flow and Heat Transfer of Non-Newtonian Tangent Hyperbolic Fluid from an Isothermal Sphere with Partial Slip

S. Abdul Gaffar · V. Ramachandra Prasad · E. Keshava Reddy · O. Anwar Bég

Received: 4 September 2013 / Accepted: 28 February 2014 / Published online: 4 September 2014

Abstract An analysis is presented for the nonlinear steady boundary layer flow and heat transfer of an incompressible Tangent Hyperbolic non-Newtonian fluid from an isothermal sphere in the presence of thermal and hydrodynamic slip condition. The transformed conservation equations are solved numerically subject to physically appropriate boundary conditions using a second-order accurate implicit finite difference Keller-box technique. The numerical code is validated with previous studies. The influence of a number of emerging non-dimensional parameters, namely the Weissenberg number (W_e), the power law index (n), Velocity slip (S_f), thermal jump (S_T), Prandtl number (Pr) and dimensionless tangential coordinate (ξ) on velocity and temperature evolution in the boundary layer regime are examined in detail. Furthermore, the effects of these parameters on *surface heat transfer rate* and *local skin friction* are also investigated. Validation with earlier *Newtonian* studies is presented and excellent correlation achieved. It is observed that velocity, skin friction and the Nusselt number (heat transfer rate) are reduced with increasing (W_e), whereas the temperature is enhanced. Increasing power (n) enhances velocity and Nusselt number (heat transfer rate) but reduces temperature and skin friction. An increase in S_f, is observed to enhance velocity and Nusselt number but reduces temperature and local skin friction. Whereas increasing S_T is found to decrease velocity, temperature, skin friction and Nusselt number. The study is relevant to chemical materials processing applications.

Keywords Non-Newtonian · Tangent hyperbolic fluid · Skin friction · Nusselt number · Weissenberg number · The power law index

S. Abdul Gaffar · E. Keshava Reddy
Department of Mathematics, Jawaharlal Nehru Technological University Anantapuram, Anantapuram 515002, India

V. Ramachandra Prasad (✉)
Department of Mathematics, Madanapalle Institute of Technology and Science, Madanapalle 517325, India
e-mail: rcpmaths@gmail.com

O. Anwar Bég
Gort Engovation Research (Aerospace), 15 Southmere Avenue, Great Horton, Bradford, BD7 3NU West Yorkshire, UK

الخلاصة

يتم في هذه الورقة العلمية عرض تحليل للتدفق غير الخطي ذي طبقة حدود ثابتة، ونقل الحرارة من سائل غير نيوتوني مغرق ، تماسي غير قابل للانضغاط من مجال متساوي الحرارة في وجود حالة الانزلاق الحراري والهيدروديناميكي. وتم حل معادلات الحفظ المحولة عدديا المتوقفة على شروط الحدود المناسبة باستخدام تقنية صندوق كيلر الدقيقة وضمنية الفروق المحدودة من الدرجة الثانية. وتم التحقق من صحة الرمز العددي مع الدراسات السابقة. وكذلك تم بالتفصيل فحص تأثير عدد من المعلمات غير البعدية الناشئة هي: عدد وينزبرغ ، ومؤشر قوة القانون ، وسرعة الانزلاق ، والقفز الحراري، وعدد برانتدل والمحاور التماسية غير البعدية على السرعة ودرجة الحرارة في تطور نظام الطبقة الحدودية. وأكثر من ذلك، فقد تم أيضا التحقيق في تأثيرات هذه المعايير في معدل نقل الحرارة السطحي واحتكاك الجلد المحلي. وتم عرض التحقق من الصحة مع الدراسات النيوتونية السابقة والحصول على ترابط ممتاز. ولوحظ أن السرعة ، واحتكاك الجلد وعدد نسلت (معدل نقل الحرارة) تنخفض مع زيادة عدد وينزبرغ ، في حين تم تعزيز درجة الحرارة. إن زيادة مؤشر قوة القانون يعزز من السرعة وعدد نسلت (معدل نقل الحرارة)، ولكن يقلل من درجة الحرارة واحتكاك الجلد. ولوحظ أن الزيادة في سرعة الانزلاق تعزز السرعة وعدد نسلت ولكنها تقلل من درجة الحرارة واحتكاك الجلد المحلي. في حين وجد أن زيادة القفز الحراري تخفض السرعة ، ودرجة الحرارة ، واحتكاك الجلد وعدد نسلت. إن هذه الدراسة هي ذات صلة بتطبيقات معالجة المواد الكيميائية.

List of symbols

a	Radius of the sphere
C_f	Skin friction coefficient
f	Non-dimensional steam function
Gr	Grashof number
g	Acceleration due to gravity
k	Thermal conductivity of fluid
K_0	Thermal jump factor
n	Power law index
Nu	Local Nusselt number
N_0	Velocity slip factor
Pr	Prandtl number
$r(x)$	Radial distance from symmetrical axis to surface of the sphere surface of the sphere
S_f	Non-dimensional Velocity slip parameter
S_T	Non-dimensional Thermal jump parameter
T	Temperature of the fluid
u, v	Non-dimensional velocity components along the x- and y-directions, respectively
V	Velocity vector
W_e	Weissenberg number
x	Streamwise coordinate
y	Transverse coordinate

Greek

α	Thermal diffusivity
β	The coefficient of thermal expansion
η	The dimensionless radial coordinate
μ	Dynamic viscosity
ν	Kinematic viscosity
θ	Non-dimensional temperature
ρ	Density of non-Newtonian fluid
ξ	The dimensionless tangential coordinate
ψ	Dimensionless stream function
Γ	Time-dependent material constant
Π	Second invariant strain tensor

Subscripts

w	Conditions at the wall (sphere surface)
∞	Free stream conditions

1 Introduction

The dynamics of non-Newtonian fluids have been a popular area of research owing to ever-increasing applications in chemical and process engineering. Examples of such fluids include coal-oil slurries, shampoo, paints, clay coating and suspensions, grease, cosmetic products, custard, physiological liquids (blood, bile and synovial fluid), etc. The classical equations employed in simulating Newtonian viscous flows, i.e., the Navier–Stokes equations fail to simulate a number of critical characteristics of non-Newtonian fluids. Hence, several constitutive equations of non-Newtonian fluids have been presented over the past decades. The relationship between the shear stress and rate of strain in such fluids are very complicated in comparison to viscous fluids. The viscoelastic features in non-Newtonian fluids add more complexities in the resulting equations when compared with Navier–Stokes equations. Significant attention has been directed at mathematical and numerical simulation of non-Newtonian fluids. Recent investigations have implemented, respectively, the Casson model [1], second-order Reiner–Rivlin differential fluid models [2], power-law nanoscale models [3], Eringen micro-morphic models [4] and Jefferys viscoelastic model [5].

Slip effects have shown to be significant in certain industrial thermal problems and manufacturing fluid dynamic systems. Sparrow et al. [6] presented the first significant investigation of laminar slip-flow heat transfer for tubes with uniform heat flux. Inman [7] further described the thermal convective slip flow in a parallel plate channel or a circular tube with uniform wall temperature. These studies generally indicated that velocity slip acts to enhance heat transfer, whereas temperature jump depresses heat transfer. Many studies have appeared in recent years considering both hydrodynamic and thermal jump effects. Interesting articles of relevance to process mechanical engineering include Larrode et al. [8] who studied thermal/velocity slip effects in conduit thermal convection. Spillane [9] who examined sheet processing boundary layer flows with slip boundary conditions and Crane and McVeigh [10] who studied slip hydrodynamics on a micro-scale cylindrical body. Further studies in the context of materials processing include Ameel et al. [11], Yu and Ameel [12], Crane and McVeigh [13]. Studies of slip flows from curved bodies include Bég et al. [14] who examined using network numerical simulation the magneto-convective slip flow from a rotating disk, Wang and Ng [15] who studied using asymptotic analysis the slip hydrodynamics from a stretching cylinder. Results assuming that the slip solution was a perturbation of the no-slip solution predicted that the slip conditions would not affect shear stress, boundary layer thickness, or heat transfer [16,17]. In addition, semi-analytic results suggested that heat transfer would change in the presence of slip flow [18–20]. Additional computations proved that shear stress would as well change [21,22]. Several explanations were offered for the contradictory results. The solutions to other viscous flows considered similar to boundary layer flows, such as Couette, Poiseuille and Rayleigh flows, showed a change in heat transfer and shear stress [23]. This led to the suggestion that the mathematical and experimental techniques available at the time lacked the accuracy necessary to capture the result. The suggestion was also made that the boundary layer equations were not valid for slip flows. Two separate arguments were made. The first was that the

second-order slip boundary condition was of the same order as the terms that were discarded from the Navier–Stokes equations to create the boundary layer equations [24,25]. A second problem was the Reynolds number scaling of the boundary layer equations. Using the definitions of viscosity and the speed of sound, the Knudsen number can be found as a function of the Mach number and Reynolds number [26]:

$$Kn_x \alpha \frac{M}{Re_x} \quad \text{(I)}$$

This scaling indicates that an incompressible boundary layer, with a Reynolds number of 500 or greater and a Mach number of <0.3, is unlikely to have a Knudsen number large enough for slip to appear. Several decades after these initial results, the development of microelectromechanical systems led to a renewed interest in slip flows [27,28]. The correct scaling of z slip was shown to be based on the boundary layer thickness and was computed as

$$Kn_\delta \alpha \frac{M}{Re_x} \quad \text{(II)}$$

This scaling does allow an incompressible boundary layer with a Reynolds number of 500 or greater and a Mach number of <0.3 to have a large enough Knudsen number for slip to appear.

An interesting non-Newtonian model developed for chemical engineering systems is the tangent hyperbolic fluid model. This rheological model has certain advantages over the other non-Newtonian formulations, including simplicity, ease of computation and physical robustness. Furthermore, it is deduced from kinetic theory of liquids rather than the empirical relation. Several communications utilizing the tangent hyperbolic fluid model have been presented in the scientific literature. There is no single non-Newtonian model that exhibits all the properties of non-Newtonian fluids. Among several non-Newtonian fluids, hyperbolic tangent model is one of the non-Newtonian models presented by Pop and Ingham [29]. Nadeem et al. [30] made a detailed study on the peristaltic transport of a hyperbolic tangent fluid in an asymmetric channel. Nadeem and Akram [31] investigated the peristaltic flow of a MHD hyperbolic tangent fluid in a vertical asymmetric channel with heat transfer. Akram and Nadeem [32] analyzed the influence of heat and mass transfer on the peristaltic flow of a hyperbolic tangent fluid in an asymmetric channel. Very recently, Akbar et al. [33] analyzed the numerical solutions of MHD boundary layer flow of tangent hyperbolic fluid on a stretching sheet. The flow due to stationary sphere has been deliberate because of its numerous applications in industries such as storage of chemicals and in particular, spherical geometries.

In many chemical engineering and nuclear process systems, *curvature of the vessels employed* is a critical aspect of optimizing thermal performance. Examples of curved bodies featuring in process systems include torus geometries, wavy surfaces, cylinders, cones, ellipses, oblate spheroids and in particular, spherical geometries, the latter being very popular for storage of chemicals and also batch reactor processing. Heat transfer from spheres has therefore mobilized much attention among chemical engineering researchers who have conducted both experimental and computational investigations for both Newtonian and non-Newtonian fluids. Amato and Chi [34] studied experimentally natural convection from heated spheres in water for an extensive range of Rayleigh numbers and for laminar, transitional and early turbulent flow using hot-film anemometry techniques. Liew and Adelman [35] conducted experiments on free convection heat transfer from an isothermal sphere to water and various aqueous polymer solutions (power-law fluids), elucidating the influence of flow behavior index and consistency index. Further empirical investigations were reported by Amato and Chi [36] for aqueous polymer solutions using and hot-film anemometry and Churchill [37], the latter deriving expressions for local and mean Nusselt number for natural convection from an isothermal sphere as a function of the Rayleigh and Prandtl numbers valid for laminar boundary layers. Sang and Kuang [38] used a finite difference code to simulate laminar mixed (forced and free) convection flow of an Eringen micropolar fluid from a permeable sphere with surface suction/injection effects. Jia [39] analyzed computationally the steady free convection from a sphere for an extensive range of Grashof (buoyancy) numbers, identifying a mushroom-shaped plume which was observed to detract in length and thickness with increasing Grashof number. He further computed flow separation at high Grashof number and an associated recirculation vortex arising in the wake of the sphere. Furthermore, this study showed that local Nusselt number along the sphere surface initially falls, attaining a minimum, and thereafter rises markedly in the vicinity of sphere rear. Sharma and Bhatnagar [40] used the Van Dyke method of matched asymptotic expansions to obtain solutions for creeping heat transfer (viscous-dominated flow) from a spherical body to power-law fluids. Bég et al. [41] examined the free convection magnetohydrodynamic flow from a sphere in porous media using network simulation, showing that temperatures are boosted with magnetic field and heat transfer is enhanced from the lower stagnation point toward the upper stagnation point. Potter and Riley [42] used a perturbation expansion approach to evaluate analytically the eruption of boundary layer into plume arising from free convection boundary layers on a sphere with strong buoyancy effects. Prhashanna and Chhabra [43] obtained numerical solutions for streamline and temperature contours in heat transfer from a heated sphere immersed in quiescent power-law fluids, showing that shear-thinning behavior may elevate heat transfer rates by three hundred percent, whereas shear-thickening depletes heat transfer rates by

30 to 40% compared with Newtonian fluids. Further interesting investigations of heat transfer from spheres have been presented by Chen and Chen [44] for power-law fluids in porous media, Dhole et al. [45] for forced convection in power-law fluids using the finite volume method and by Bég et al. [46] for combined heat and species diffusion in micropolar fluids with cross-diffusion effects. Prasad et al. [47] have also studied radiative heat flux effects on magneto-convective heat and species diffusion from a sphere in an isotropic permeable medium.

The objective of the present study is to investigate the laminar boundary layer flow and heat transfer of a *tangent hyperbolic* non-Newtonian fluid from an isothermal sphere. The non-dimensional equations with associated dimensionless boundary conditions constitute a highly nonlinear, coupled two-point boundary value problem. Keller's implicit finite difference "box" scheme is implemented to solve the problem [47]. The effects of the emerging thermophysical parameters, namely*the Weissenberg number* (W_e), *power law index (n), Thermal jump* (S_T), *Velocity slip* (S_f) *and Prandtl number (Pr),* on the velocity, temperature, skin friction number, and heat transfer rate (local Nusselt number) characteristics are studied. The present problem has to the authors' knowledge not appeared thus far in the scientific literature and is relevant to polymeric manufacturing processes in chemical engineering.

2 Non-Newtonian Constitutive Tangent Hyperbolic Fluid Model

In the present study, a subclass of non-Newtonian fluids known as the *tangent hyperbolic fluid* is employed owing to its simplicity. The Cauchy stress tensor, in the *tangent hyperbolic* non-Newtonian fluid [29] takes the form:

$$\overline{\tau} = \left[\mu_\infty + (\mu_0 + \mu_\infty)\tanh\left(\Gamma\overline{\dot{\gamma}}\right)^n\right]\overline{\dot{\gamma}} \tag{1}$$

where $\bar{\tau}$ is extra stress tensor, μ_∞ is the infinite shear rate viscosity, μ_0 is the zero shear rate viscosity, Γ is the time-dependent material constant, n is the power law index, i.e., flow behavior index and $\overline{\dot{\gamma}}$ is defined as

$$\overline{\dot{\gamma}} = \sqrt{\frac{1}{2}\sum_i\sum_j \overline{\dot{\gamma}}_{ij}\overline{\dot{\gamma}}_{ji}} = \sqrt{\frac{1}{2}\Pi}, \tag{2}$$

where $\Pi = \frac{1}{2}trac\left(gradV + (gradV)^T\right)^2$. We consider Eq. (1), for the case when $\mu_\infty = 0$ because it is not possible to discuss the problem for the infinite shear rate viscosity and since we considering tangent hyperbolic fluid that describing shear thinning effects so $\Gamma\overline{\dot{\gamma}} < 1$. Then Eq. (1) takes the form

$$\begin{aligned}\overline{\tau} &= \mu_0\left[\left(\Gamma\overline{\dot{\gamma}}\right)^n\right]\overline{\dot{\gamma}} = \mu_0\left[\left(1+\Gamma\overline{\dot{\gamma}}-1\right)^n\right]\overline{\dot{\gamma}}\\ &= \mu_0\left[1+n\left(\Gamma\overline{\dot{\gamma}}-1\right)\right]\overline{\dot{\gamma}}\end{aligned} \tag{3}$$

The introduction of the appropriate terms into the flow model is considered next. The resulting boundary value problem is found to be well posed and permits an excellent mechanism for the assessment of rheological characteristics on the flow behavior.

3 Mathematical Flow Model

Steady, double-diffusive, laminar, incompressible flow of a tangent hyperbolic fluid from an isothermal sphere is considered, as illustrated in Fig. 1. The x-coordinate (tangential) is measured along the surface of the isothermal sphere from the lowest point and the y-coordinate (radial) is directed

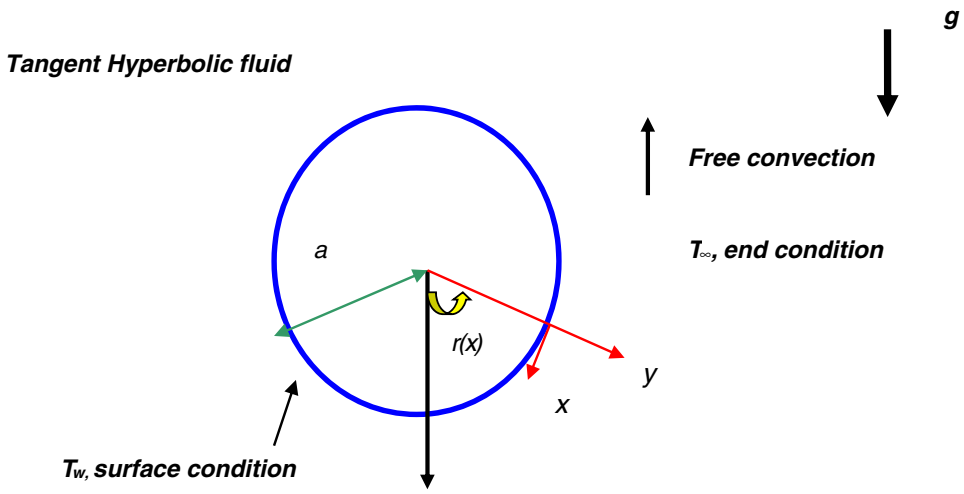

Fig. 1 Physical model and coordinate system

Table 1 Values of $f''(\xi,0)$ and $-\theta'(\xi,0)$ for different values of S_f, S_T and ξ ($Pr = 7.0$, $W_e = 0.3$, $n = 0.3$)

S_f	S_T	$\xi = 0.0$		$\xi = \pi/6$		$\xi = \pi/4$		$\xi = \pi/3$	
		$f''(\xi,0)$	$-\theta'(\xi,0)$	$f''(\xi,0)$	$-\theta'(\xi,0)$	$f''(\xi,0)$	$-\theta'(\xi,0)$	$f''(\xi,0)$	$-\theta'(\xi,0)$
0.0	1.0	0	0.7163	0.1672	0.7007	0.2285	0.6871	0.3099	0.6583
0.1		0	0.7374	0.1620	0.7215	0.2213	0.7076	0.3000	0.6782
0.2		0	0.7584	0.1568	0.7422	0.2141	0.7280	0.2900	0.6981
0.3		0	0.7793	0.1516	0.7629	0.2069	0.7485	0.2800	0.7180
0.5		0	0.8212	0.1409	0.8042	0.1921	007893	0.2596	0.7577
0.8		0	0.8835	0.1246	0.8656	0.1696	0.8499	0.2284	0.8166
1.0		0	0.9246	0.1135	0.9061	0.1543	0.8899	0.2071	0.8555
0.5	0.0	0	1.1559	0.1772	1.1318	0.2418	1.1107	0.3272	1.0660
	0.5	0	0.9860	0.1595	0.9656	0.2175	0.9476	0.2941	0.9095
	1.5	0	0.6619	0.1214	0.6683	0.1654	0.6363	0.2234	0.6109
	2.0	0	0.5090	0.1007	0.4986	0.1372	0.4894	0.1850	0.4699
	2.5	0	0.3636	0.0785	0.3562	0.1068	0.3497	0.1439	0.3359
	3.0	0	0.2273	0.0543	0.2228	0.0738	0.2187	0.0991	0.2102

Table 2 Values of $f''(\xi,0)$ and $-\theta'(\xi,0)$ for different values of S_f, S_T and ξ ($Pr = 7.0$, $W_e = 0.3$, $n = 0.3$)

S_f	S_T	$\xi = \pi/2$		$\xi = 2\pi/3$		$\xi = \pi$	
		$f''(\xi,0)$	$-\theta'(\xi,0)$	$f''(\xi,0)$	$-\theta'(\xi,0)$	$f''(\xi,0)$	$-\theta'(\xi,0)$
0.0	1.0	0.4071	0.5865	0.4402	0.4795	0.4412	0.3932
0.1		0.3935	0.6048	0.4247	0.4946	0.4250	0.4052
0.2		0.3798	0.6230	0.4090	0.5697	0.4090	0.4171
0.3		0.3660	0.6412	0.3930	0.5248	0.3931	0.4291
0.5		0.3379	0.6775	0.3606	0.5548	0.3612	0.4531
0.8		0.2946	0.7314	0.3105	0.5994	0.3119	0.4888
1.0		0.2651	0.7669	0.2761	0.6288	0.2781	0.5933
0.5	0.0	0.4270	0.9530	0.4576	0.7803	0.4579	0.6376
	0.5	0.3834	0.8132	0.4101	0.6659	0.4105	0.5439
	1.5	0.2901	0.5464	0.3088	0.4475	0.3095	0.3653
	2.0	0.2397	0.4205	0.2542	0.3444	0.2550	0.2810
	2.5	0.1858	0.3006	0.1961	0.2463	0.1969	0.2009
	3.0	0.1272	0.1883	0.1331	0.1543	0.1339	0.1456

perpendicular to the surface, with a denoting the radius of the isothermal sphere. $r(x) = a\sin(x/a)$ is the radial distance from the symmetrical axis to the surface of the sphere. The gravitational acceleration $\boldsymbol{g}$, acts downwards. We also assume that the Boussineq approximation holds, i.e., that density variation is only experienced in the buoyancy term in the momentum equation.

Both isothermal sphere and the tangent hyperbolic fluid are maintained initially at the same temperature. Instantaneously, they are raised to a temperature $T_w > T_\infty$, the ambient temperature of the fluid which remains unchanged. In line with the approach of Yih [48] and introducing the boundary layer approximations, the equations for *mass, momentum and energy*, can be written as follows:

$$\frac{\partial u}{\partial x} + \frac{\partial v}{\partial y} = 0 \tag{4}$$

$$u\frac{\partial u}{\partial x} + v\frac{\partial u}{\partial y} = \nu(1-n)\frac{\partial^2 u}{\partial y^2} + \sqrt{2}\nu n\Gamma\left(\frac{\partial u}{\partial y}\right)\frac{\partial^2 u}{\partial y^2} + g\beta\sin\left(\frac{x}{a}\right)(T - T_\infty) \tag{5}$$

$$u\frac{\partial T}{\partial x} + v\frac{\partial T}{\partial y} = \alpha\frac{\partial^2 T}{\partial y^2} \tag{6}$$

where u and v are the velocity components in the x- and y-directions, respectively, is the $\nu = \mu/\rho$ kinematic viscosity of the tangent hyperbolic fluid, β is the coefficient of thermal expansion, α is the thermal diffusivity, T is the temperature, ρ is the density of the fluid. The tangent hyperbolic fluid

Table 3 Values of $f''(\xi,0)$ and $-\theta'(\xi,0)$ for different values of W_e, n and Pr ($S_f = 0.5,\ S_T = 1.0,\ \xi = 1.0$)

W_e	N	$Pr = 7$		$Pr = 10$		$Pr = 20$		$Pr = 25$	
		$f''(\xi,0)$	$-\theta'(\xi,0)$	$f''(\xi,0)$	$-\theta'(\xi,0)$	$f''(\xi,0)$	$-\theta'(\xi,0)$	$f''(\xi,0)$	$-\theta'(\xi,0)$
0.0	0.3	0.2714	0.7592	0.2465	0.8650	0.2006	1.1202	0.1866	1.2202
0.5		0.2523	0.7567	0.2306	0.8624	0.1898	1.1178	0.1772	1.2178
1.0		0.2355	0.7543	0.2164	0.8600	0.1800	1.1155	0.1686	1.2156
2.0		0.2067	0.7501	0.1920	0.8557	0.1628	1.1113	0.1534	1.2115
3.0		0.1829	0.7463	0.1715	0.8518	0.1481	1.1075	0.1403	1.2079
4.0		0.1625	0.7430	0.1538	0.8484	0.1352	1.1041	0.1288	1.2045
5.0		0.1447	0.7400	0.1383	0.8452	0.1238	1.1009	0.1186	1.2014
0.3	0.0	0.2945	0.7235	0.2657	0.8256	0.2131	1.0748	0.1971	1.1734
	0.1	0.2849	0.7335	0.2578	0.8366	0.2080	1.0874	0.1928	1.1863
	0.2	0.2735	0.7448	0.2483	0.8490	0.2018	1.1018	0.1875	1.2012
	0.4	0.2422	0.7726	0.2220	0.8802	0.1839	1.1388	0.1720	1.2397
	0.5	0.2198	0.7901	0.2028	0.9001	0.1703	1.1631	0.1600	1.2652
	0.6	0.1894	0.8112	0.1764	0.9243	0.1511	1.1932	0.1430	1.2970

Table 4 Values of $f''(\xi,0)$ and $-\theta'(\xi,0)$ for different values of W_e, n and Pr ($S_f = 0.5,\ S_T = 1.0, \xi = 1.0$)

W_e	N	$Pr = 50$		$Pr = 75$		$Pr = 100$	
		$f''(\xi,0)$	$-\theta'(\xi,0)$	$f''(\xi,0)$	$-\theta'(\xi,0)$	$f''(\xi,0)$	$-\theta'(\xi,0)$
0.0	0.3	0.1459	1.6062	0.1242	1.9008	0.1099	2.1500
0.5		0.1400	1.6043	0.1199	1.8992	0.1065	2.1486
1.0		0.1345	1.6024	0.1158	1.8977	0.1033	2.1473
2.0		0.1246	1.5990	0.1084	1.8948	0.0973	2.1448
3.0		0.1160	1.5959	0.1018	1.8921	0.0920	2.1425
4.0		0.1082	1.5930	0.0958	1.8896	0.0871	2.1403
5.0		0.1012	1.5903	0.0904	1.8873	0.0826	2.1383
0.3	0.0	0.1513	1.5574	0.1272	1.8529	0.1116	2.1035
	0.1	0.1490	1.5707	0.1259	1.8659	0.1108	2.1160
	0.2	0.1461	1.5864	0.1241	1.8813	0.1096	2.1310
	0.4	0.1370	1.6277	0.1179	1.9227	0.1052	2.1717
	0.5	0.294	1.6560	0.1125	1.9517	0.1010	2.2006
	0.6	0.1181	1.6923	0.1040	1.9895	0.0943	2.2388

model therefore introduces a *mixed* derivative (second order, first degree) into the momentum boundary layer Eq. (5). The non-Newtonian effects feature in the shear terms only of Eq. (5) and not the convective (acceleration) terms. The third term on the right hand side of Eq. (5) represents the *thermal buoyancy force* and couples the velocity field with the temperature field Eq. (6).

$$\begin{aligned} &\text{At } y = 0, \quad u = N_0 \frac{\partial u}{\partial y}, \quad v = 0, \quad T = T_w + K_0 \frac{\partial T}{\partial y} \\ &\text{As } y \to \infty, \quad u \to 0, \quad T \to T_\infty \end{aligned} \tag{7}$$

Here N_0 is the velocity slip factor, K_0 is the thermal jump factor and T_∞ is the free stream temperature. For $N_0 = 0 = K_0$, one can recover the no-slip case.

The stream function ψ is defined by $u = \frac{\partial \psi}{\partial y}$ and $v = -\frac{\partial \psi}{\partial x}$, and therefore, the continuity equation is automatically satisfied. In order to render the governing equations and the boundary conditions in dimensionless form, the following non-dimensional quantities are introduced.

$$\begin{aligned} &\xi = \frac{x}{a}, \quad \eta = \frac{y}{a} Gr^{1/4}, \quad f = \frac{\psi}{\nu \xi} Gr^{-1/4}, \\ &\theta(\xi,\eta) = \frac{T - T_\infty}{T_w - T_\infty} \\ &\Pr = \frac{\nu}{\alpha}, \quad Gr = \frac{g\beta_1 (T_w - T_\infty) a^3}{\nu^2}, \\ &W_e = \frac{\sqrt{2}\nu \Gamma x Gr^{3/4}}{a^3}, \quad M = \frac{\sigma B_0^2 a^2}{\rho \nu \sqrt{Gr}} \end{aligned} \tag{8}$$

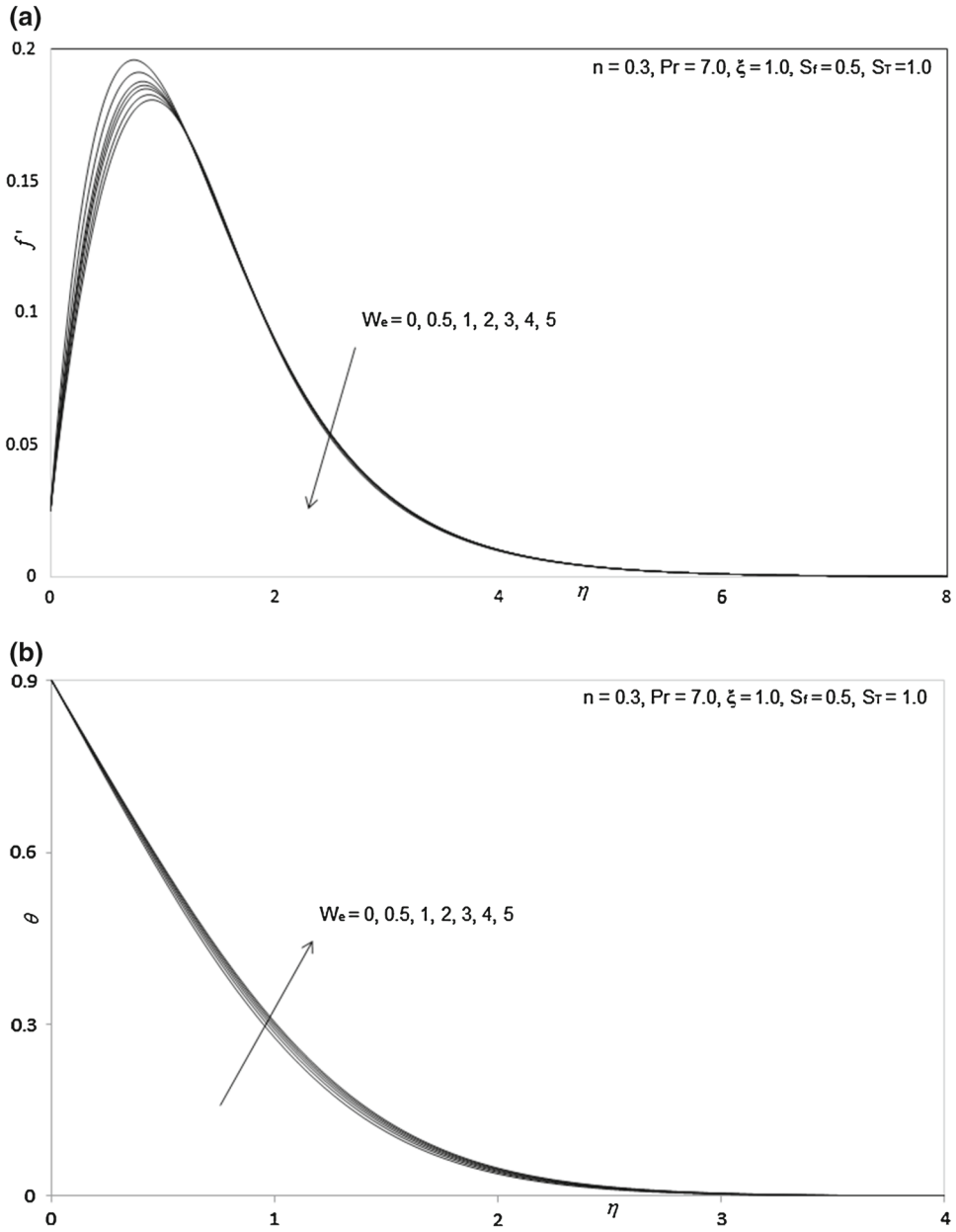

Fig. 2 **a** Influence of W_e on velocity profiles. **b** Influence of W_e on temperature profiles

All terms are defined in the nomenclature. In view of the transformation defined in Eq. (8), the boundary layer Eqs. (5)–(7) are reduced to the following coupled, nonlinear, dimensionless partial differential equations for momentum and energy for the regime:

$$(1-n)\,f''' + (1+\xi\cot\xi)\,ff'' - \left(f'\right)^2 + nW_e f''f''' + \theta\frac{\sin\xi}{\xi} = \xi\left(f'\frac{\partial f'}{\partial\xi} - f''\frac{\partial f}{\partial\xi}\right) \tag{9}$$

$$\frac{\theta''}{Pr} + (1+\xi\cot\xi)\,f\theta' = \xi\left(f'\frac{\partial\theta}{\partial\xi} - \theta'\frac{\partial f}{\partial\xi}\right) \tag{10}$$

The transformed dimensionless boundary conditions are:

$$\begin{aligned} &At \quad \eta = 0,\ f = 0,\ f' = S_f f''(0),\ \theta = 1 + S_T\theta'(0) \\ &As \quad \eta \to \infty,\ f' \to 0,\ \theta \to 0 \end{aligned} \tag{11}$$

Here, primes denote the differentiation with respect to η, $S_f = \frac{N_0 Gr^{1/4}}{a}$ and $S_T = \frac{K_0 Gr^{1/4}}{a}$ are the non-dimensional velocity slip and thermal jump parameters, respectively. The skin friction coefficient (shear stress at the sphere surface) and Nusselt number (heat transfer rate) can be defined using the transformations described above with the following expressions.

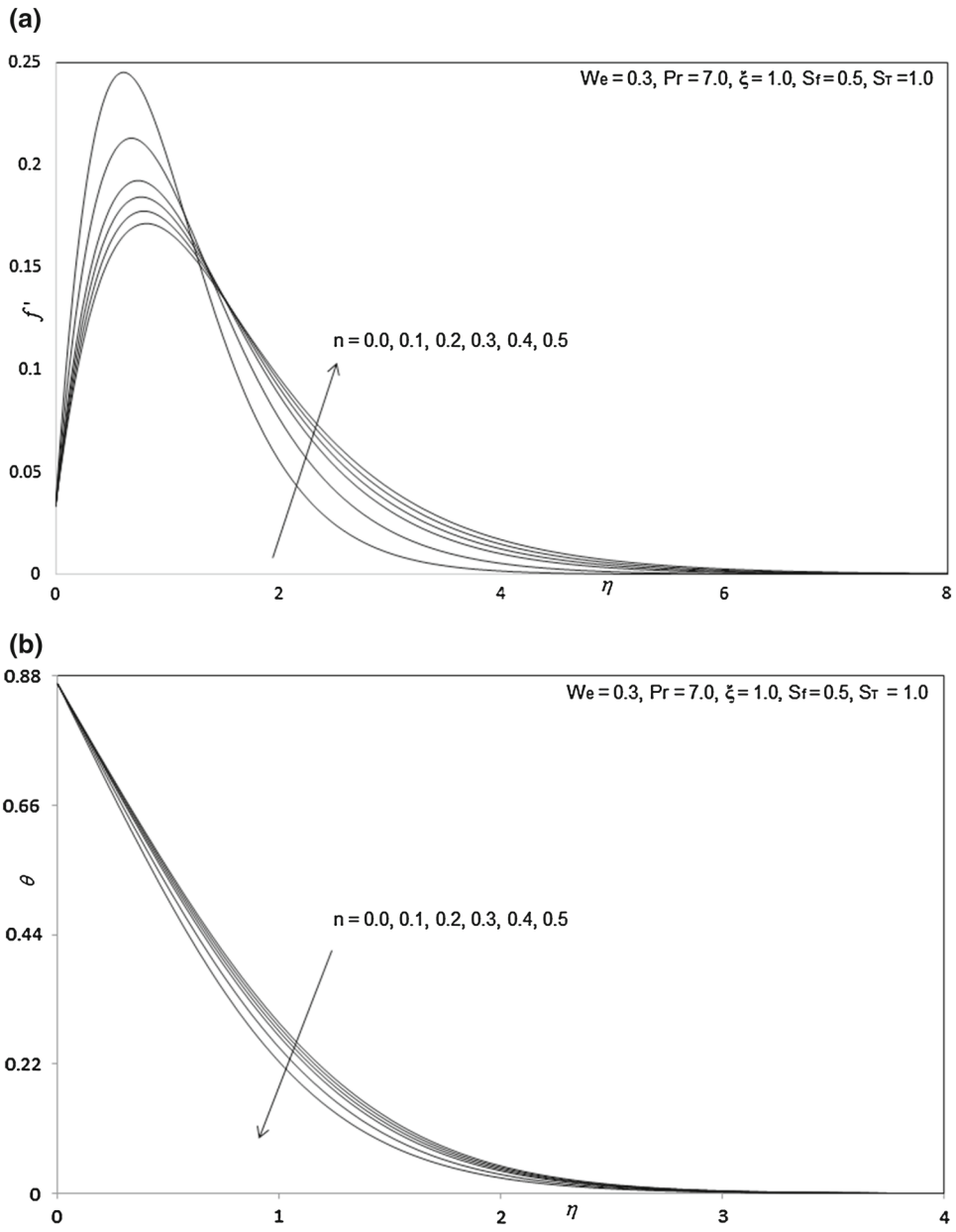

Fig. 3 **a** Influence of n on velocity profiles. **b** Influence of n on temperature profiles

$$Gr^{-3/4}C_{\mathrm{f}} = (1-n)\,\xi f''(\xi,0) + \frac{n}{2}W_e\xi\left(f''(\xi,0)\right)^2 \quad (12)$$

$$Gr^{-1/4}Nu = -\theta'(\xi,0) \quad (13)$$

The location, $\xi \sim 0$, corresponds to the vicinity of the *lower stagnation point* on the sphere.

Since $\frac{\sin\xi}{\xi} \rightarrow 0/0$, i.e., 1. For this scenario, the model defined by Eqs. (9) and (10) contracts to an *ordinary* differential boundary value problem:

$$(1-n)\,f''' + ff'' - \left(f'\right)^2 + nW_{\mathrm{e}}f''f''' + \theta = 0 \quad (14)$$

$$\frac{1}{\mathrm{Pr}}\theta'' + f\theta' = 0 \quad (15)$$

The general model is solved using a powerful and unconditionally stable finite difference technique introduced by Keller [49]. The Keller-box method has a second order accuracy with arbitrary spacing and attractive extrapolation features.

4 Numerical Solution with Keller Box Implict Method

The Keller-box implicit difference method is implemented to solve the nonlinear boundary value problem defined by Eqs. (9)–(10) with boundary conditions (11). This technique, despite recent developments in other numerical methods,

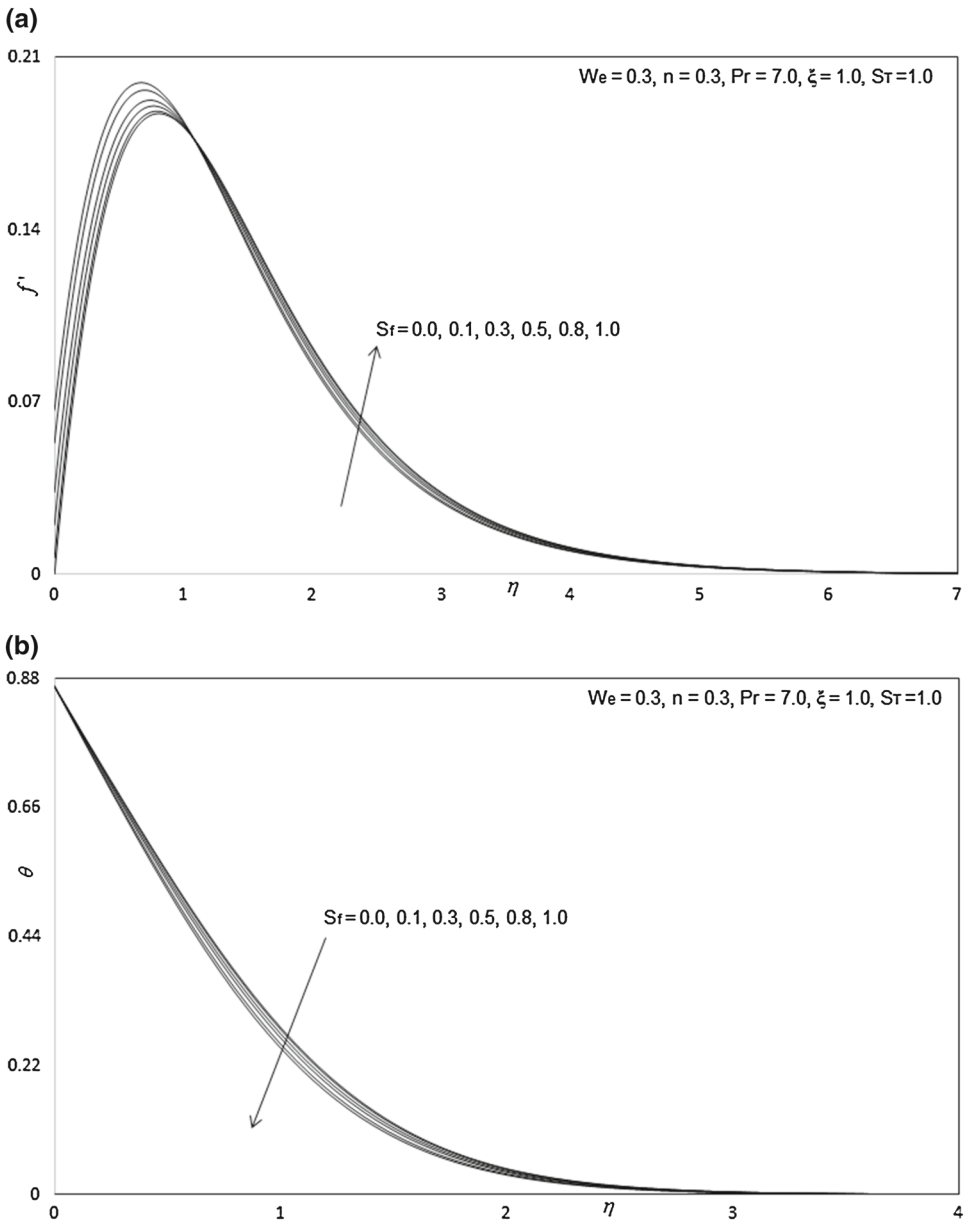

Fig. 4 **a** Influence of S_f on velocity profiles. **b** Influence of S_f on temperature profiles

remains a powerful and very accurate approach for parabolic boundary layer flows. It is unconditionally stable and achieves exceptional accuracy [49]. Recently, this method has been deployed in resolving many challenging, multi-physical fluid dynamics problems. These include hydromagnetic Sakiadis flow of non-Newtonian fluids [50], radiative rheological magnetic heat transfer [51], waterhammer modeling [52] and magnetized viscoelastic stagnation flows [53]. The Keller-box discretization is *fully coupled* at each step which reflects the physics of parabolic systems—which are also fully coupled. Discrete calculus associated with the Keller-box scheme has also been shown to be fundamentally different from all other mimetic (physics capturing) numerical methods, as elaborated by Keller [49]. The Keller-box Scheme comprises four stages.

1. Decomposition of the Nth order partial differential equation system to N first order equations.
2. Finite Difference Discretization.
3. Quasilinearization of Non-Linear Keller Algebraic Equations and finally.
4. Block-tridiagonal Elimination solution of the Linearized Keller Algebraic Equations.

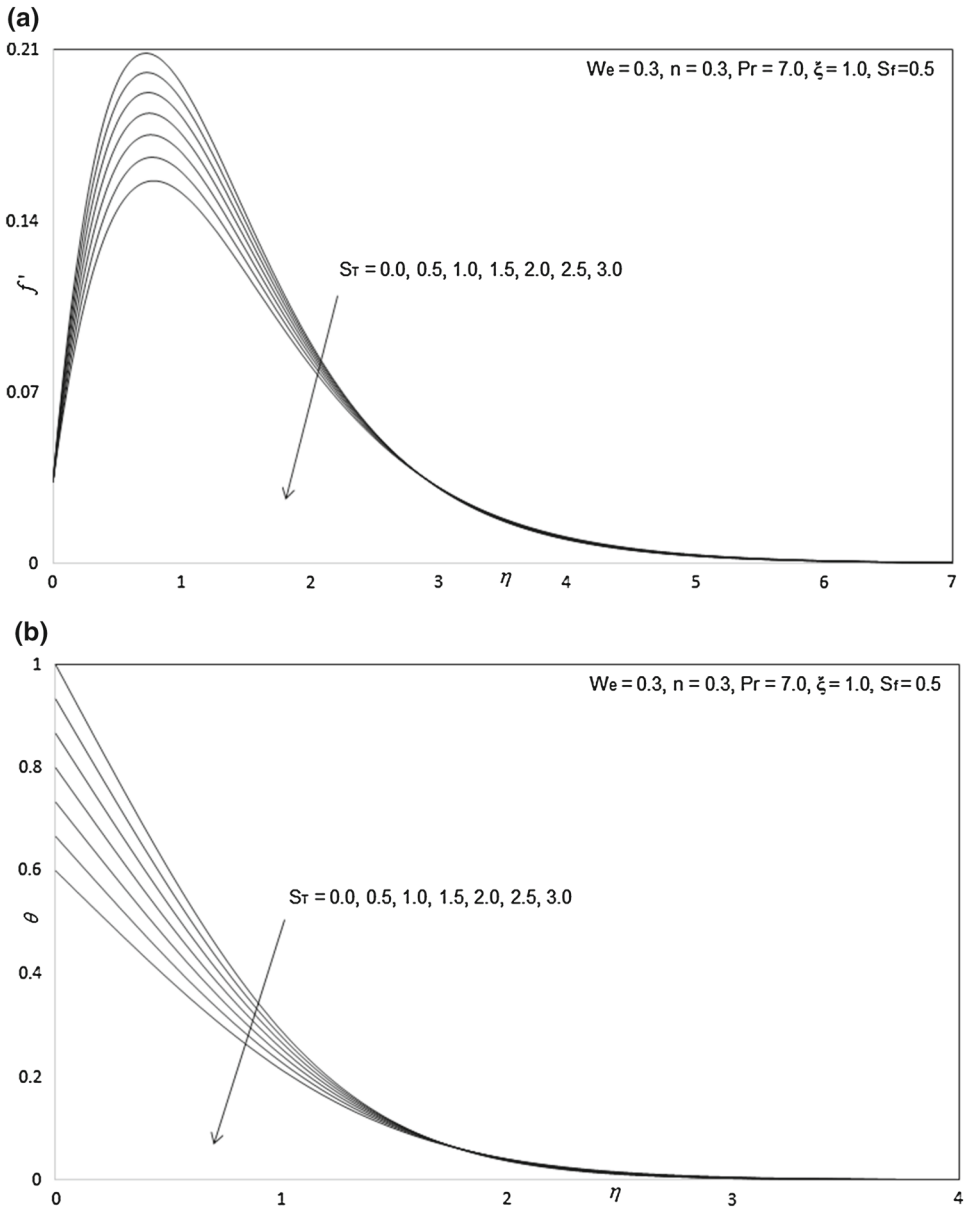

Fig. 5 **a** Influence of S_T on velocity profiles. **b** Influence of S_T on temperature profiles

Stability and Convergence of Keller-box Method

In laminar boundary layer calculations, the wall shear stress parameter $v\,(x, 0)$, is commonly used as the convergence criterion [54]. This is probably because in boundary layer calculations, it is found that the greatest error usually appears in the wall shear stress parameter. Different criterion is used for turbulent flows problem. Throughout the study of this paper, the convergence criterion is used as it is efficient, suitable and the best. Calculations are stopped when

$$\left|\delta v_0^{(i)}\right| < \varepsilon_1$$

Where ε_1 is a small prescribed value.

5 Numerical Results and Interpretation

Comprehensive solutions have been obtained and are presented in Tables 1, 2, 3 and 4 and Figs. 2, 3, 4, 5, 6, 7, 8, 9 and 10. The numerical problem comprises two independent variables (ξ, η), two dependent fluid dynamic variables (f, θ) and five thermo-physical and body force control parameters, namely W_e, n, S_f, S_T, Pr, ξ. The following default parameter values, i.e., $W_e = 0.3$, $n = 0.3$, $S_f, = 0.5$, $S_T = 1.0$, $Pr = 7.0$, $\xi = 1.0$ are prescribed (unless otherwise stated). Furthermore, the influence of streamwise (transverse) coordinate on heat transfer characteristics is also investigated.

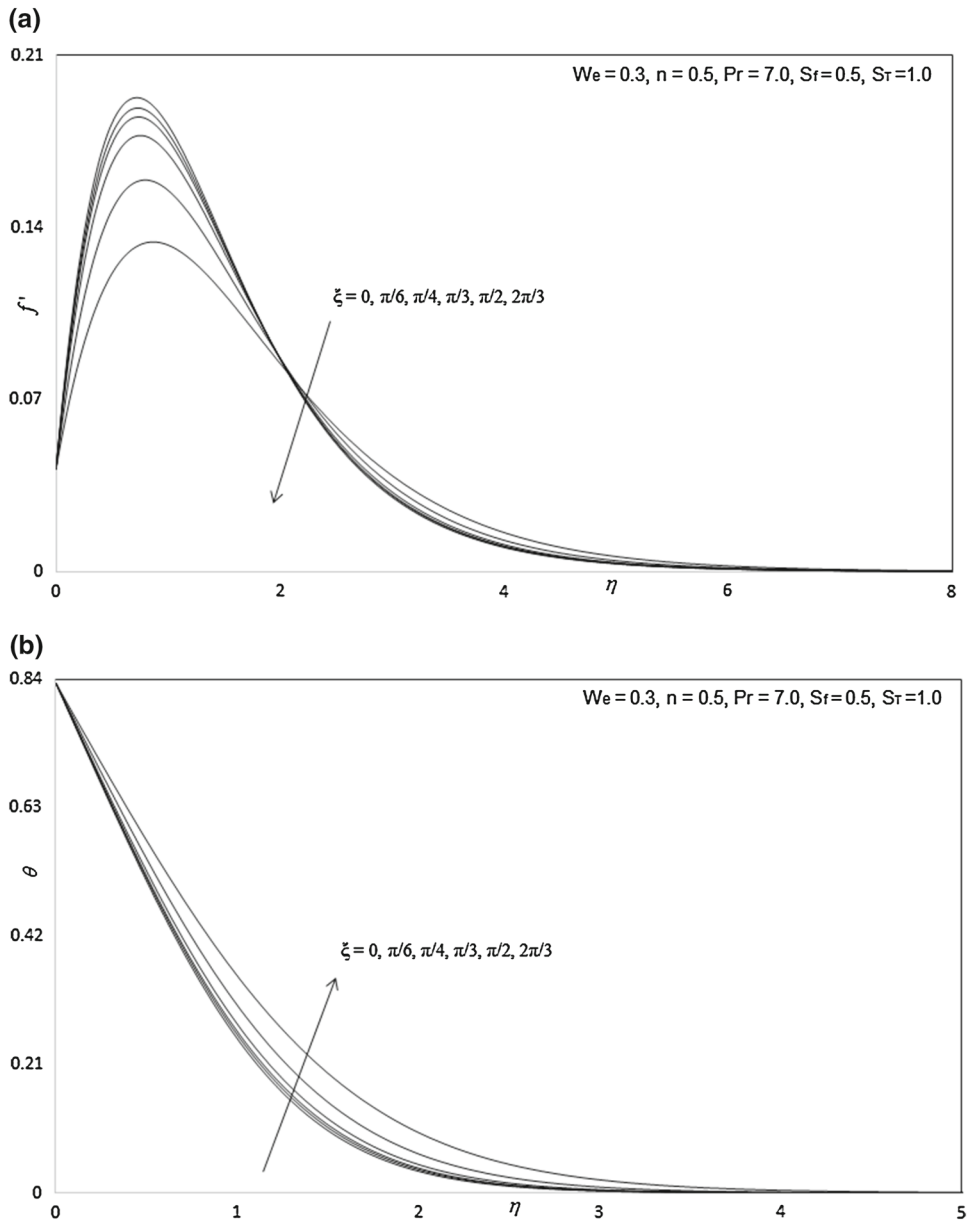

Fig. 6 **a** Influence of ξ on velocity profiles. **b** Influence of ξ on temperature profiles

In Tables 1 and 2 document results for the influence of the velocity slip (S_f) and the thermal jump (S_T) on skin friction and heat transfer rate (Nusselt number), along with a variation in the traverse coordinate (ξ). It has been observed that increasing S_f reduces skin friction but increases heat transfer rate (Nusselt numbers). Also increasing S_T is found to reduce both skin friction and heat transfer rate (Nusselt number). These tables also show that with an increase in ξ, skin friction is accelerated, whereas heat transfer rate is decelerated.

Tables 3 and 4, presents the influence of the Weissenberg number (W_e) and the power law index (n), on the skin friction and heat transfer rate (Nusselt number), along with a variation in the Prandtl number (Pr). With increasing W_e, both skin friction and heat transfer rate (Nusselt numbers) are reduced. Furthermore, an increase in the power law index (n) decreases skin friction coefficient but increases heat transfer rate. Increasing Prandtl number (Pr) reduces skin friction but enhances heat transfer rate (Nusselt number).

Figure 2a, b depict the velocity (f') and temperature (θ) distributions with increasing *Weissenberg number,* W_e. Very little tangible effect is observed in Fig. 2a, although there is a very slight decrease in velocity with increase in *We*. Conversely, there is only a very slight increase in temperature magnitudes in Fig. 2b with a rise in *We*. The mathematical model reduces to the *Newtonian viscous flow model* as $W_e \rightarrow 0$ and $n \rightarrow 0$. The momentum boundary layer equation in this case contracts to the familiar equation for *Newtonian mixed convection* from a plate, viz.

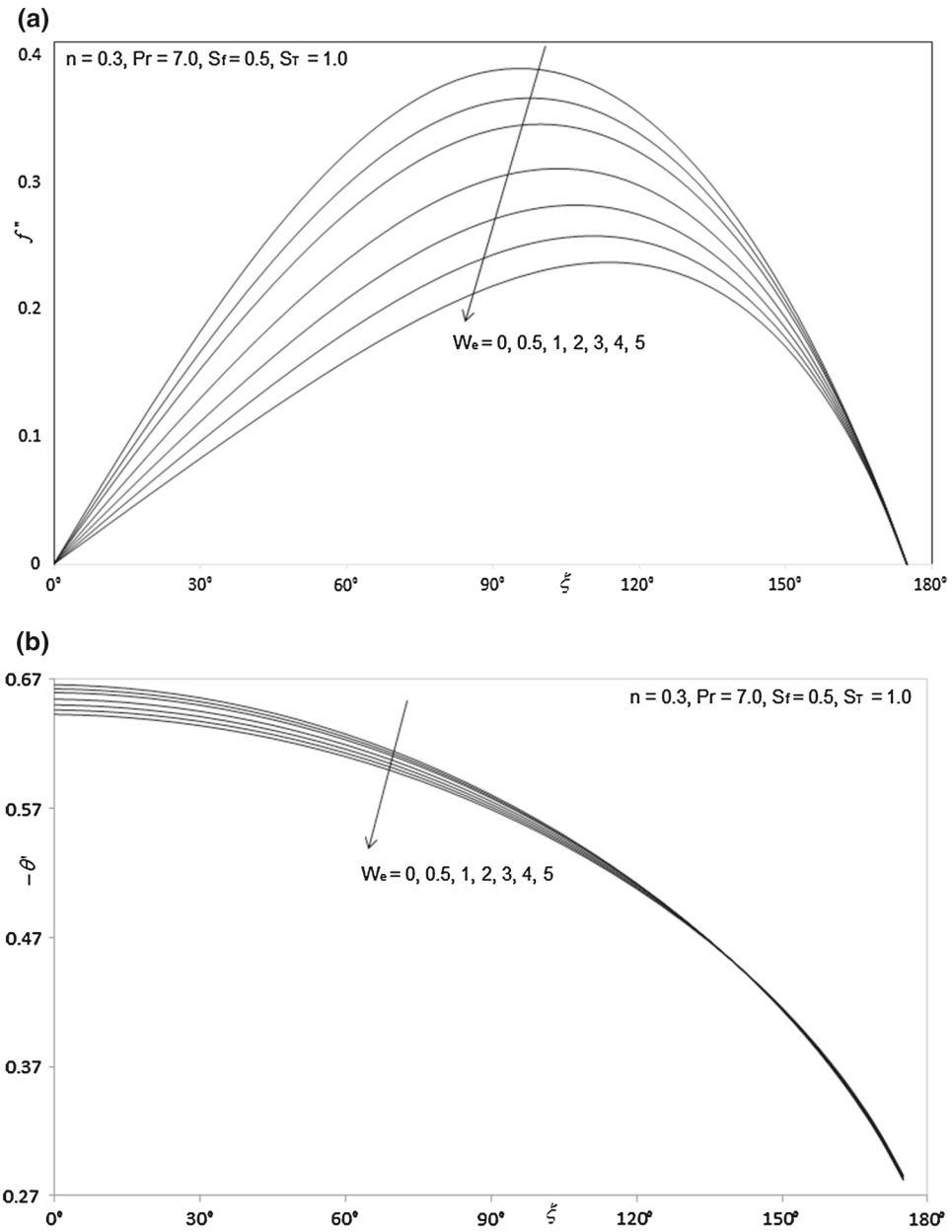

Fig. 7 **a** Influence of W_e on skin friction coefficient result. **b** Influence of W_e on Nusselt number result

$f'''+(1+\xi\cot\xi)\,ff''-f'^2+\theta\frac{\sin\xi}{\xi}=\xi\left(f'\frac{\partial f'}{\partial\xi}-f''\frac{\partial f}{\partial\xi}\right)$. The thermal boundary layer Eq. (10) remains unchanged.

Figure 3a, b illustrates the effect of the *power law index*, n, on the velocity $\left(f'\right)$ and temperature (θ) distributions through the boundary layer regime. Velocity is significantly increased with increasing n. Conversely, temperature is consistently reduced with increasing values of n.

Figure 4a, b depict the evolution of velocity $\left(f'\right)$ and temperature (θ) functions with a variation in velocity slip parameter, S_f. Dimensionless velocity component (Fig. 4a) is considerably enhanced with increasing S_f. In Fig. 4b, an increase in S_f is seen to considerably reduce temperatures throughout the boundary layer regime. The influence of S_f is evidently more pronounced closer to the sphere surface ($\eta = 0$). Further from the surface, there is a transition in *velocity slip effect*, and the flow is found to be accelerated markedly. Smooth increase in the velocity profiles are observed into the free stream demonstrating excellent convergence of the numerical solution. Furthermore, the acceleration near the wall with increasing velocity slip effect has been computed by Crane and McVeigh [13] using asymptotic methods, as has the retardation in flow further from the wall. The switch in velocity slip effect on velocity evolution has also been observed for the case of a power-law rheological fluid by O.Ajadi et al. [57]. Figure 4b shows that an increase in S_f, significantly reduces temperature. Tempera-

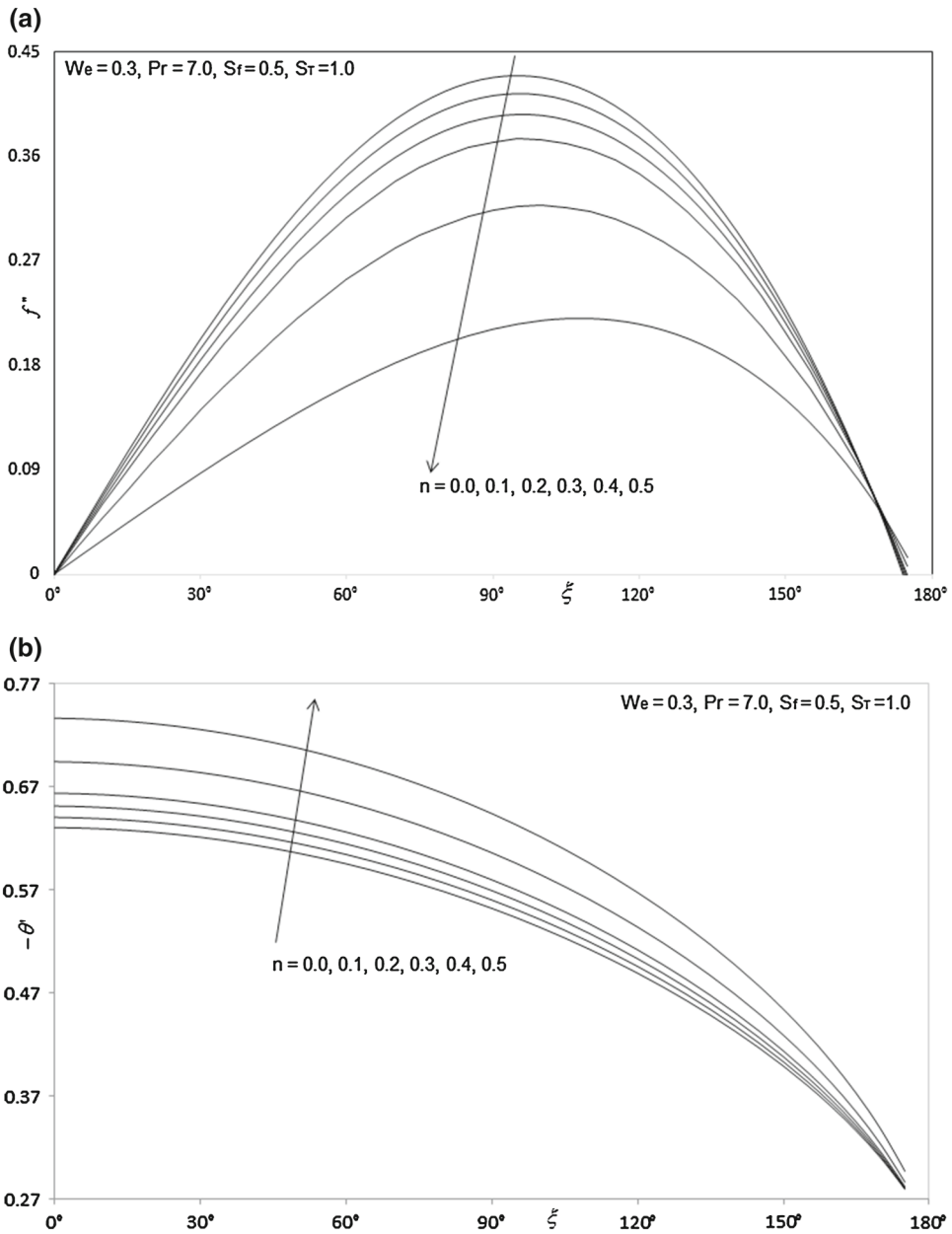

Fig. 8 **a** Influence of n on skin friction coefficient result. **b** Influence of n on Nusselt number result

ture profiles consistently decay monotonically from a maximum at the sphere surface to the free stream. All profiles converge at large value of radial coordinate, again showing that convergence has been achieved in the numerical computations.

Figure 5a, b depict the evolution of velocity $\left(f'\right)$ and temperature (θ) functions with a variation in thermal jump parameter, S_{T}. The response of velocity is much more consistent than for the case of changing velocity slip parameter (Fig. 4a). It is strongly decreased for all locations in the radial direction. The peak velocity accompanies the case of no thermal jump ($S_{\mathrm{T}} = 0$). The maximum deceleration corresponds to the case of strongest thermal jump ($S_{\mathrm{T}} = 3$). Temperatures (Fig. 5b) are also strongly depressed with increasing thermal jump. The maximum effect is observed at the wall. Further into the free stream, all temperature profiles converge smoothly to the vanishing value. The numerical computations correlate well with the results of Larrode et al. [8] who also found that temperature is strongly lowered with increasing thermal jump and that this is attributable to the decrease in heat transfer from the wall to the fluid regime, although they considered only a Newtonian fluid.

Figure 6a, b depict the velocity $\left(f'\right)$ and temperature (θ) distributions with dimensionless radial coordinate, for various transverse (streamwise) coordinate values, ξ. Generally, velocity is noticeably lowered with increasing migra-

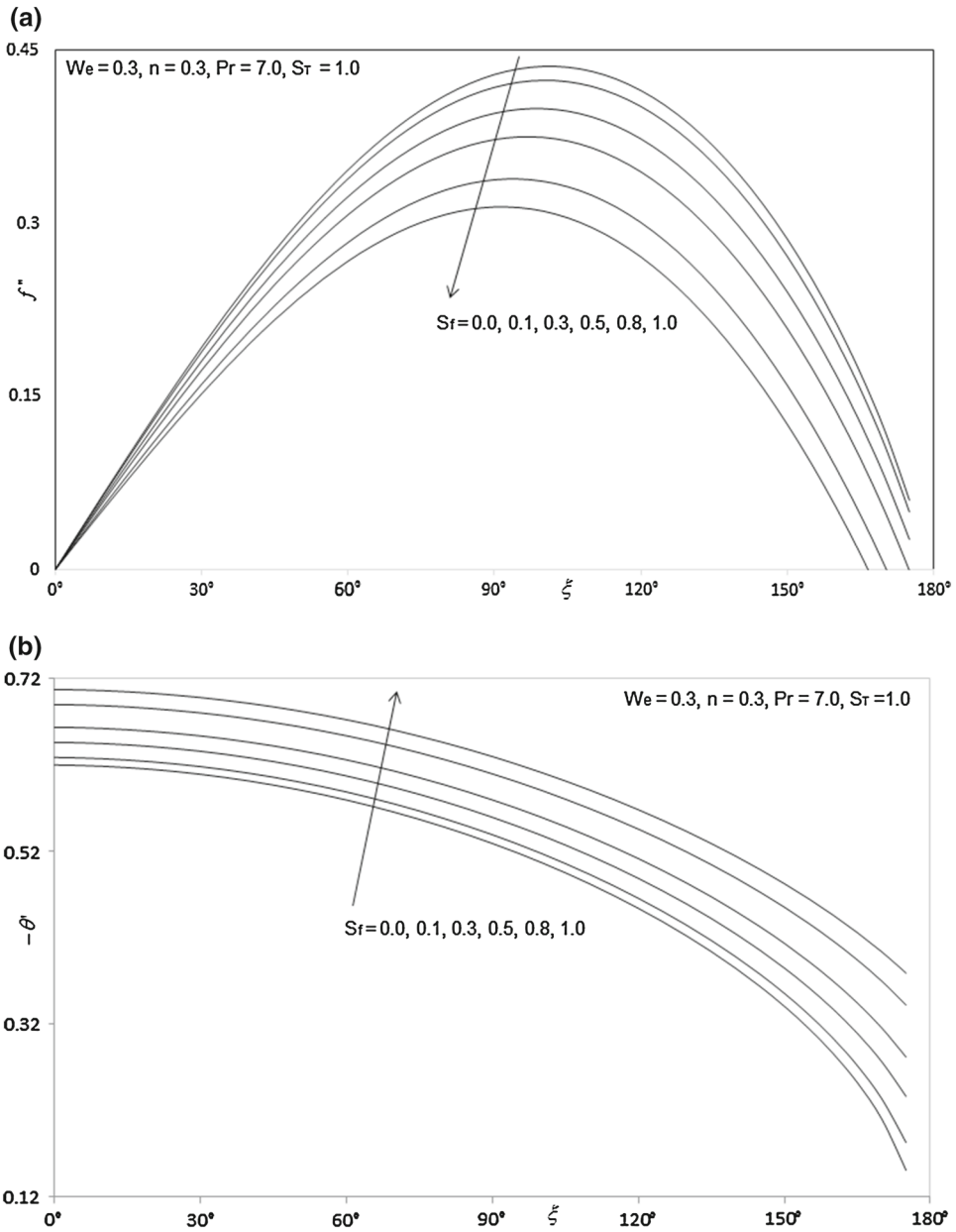

Fig. 9 **a** Influence of S_f on skin friction coefficient result. **b** Influence of S_f on Nusselt number result

tion from the leading edge, i.e., larger ξ values (Fig. 6a). The maximum velocity is computed at the *lower stagnation point* ($\xi \sim 0$) for *low values* of radial coordinate (η). The transverse coordinate clearly exerts a significant influence on momentum development. A very strong increase in temperature (θ), as observed in Fig. 6b, is generated throughout the boundary layer with increasing ξ values. The temperature field *decays monotonically*. Temperature is maximized at the surface of the spherical body ($\eta = 0$, for all ξ) and minimized in the free stream ($\xi = 25$). Although the behavior at the upper stagnation point ($\xi \sim \pi$) is not computed, the pattern in Fig. 6b suggests that temperature will continue to progressively grow here compared with previous locations on the sphere surface (lower values of ξ).

Figure 7a, b show the influence of Weissenberg number, W_e, on the dimensionless skin friction coefficient $\left((1-n)\,\xi f''(\xi,0) + \frac{nW_e}{2}\xi\left(f'\prime(\xi,0)\right)^2\right)$ and heat transfer rate $\left(\theta'(\xi,0)\right)$ at the sphere surface. It is observed that the dimensionless skin friction is decreased with the increase in W_e, i.e., the boundary layer flow is accelerated with decreasing viscosity effects in the non-Newtonian regime. The surface heat transfer rate is also substantially *decreased* with increasing W_e values.

Figure 8a, b illustrates the influence of the power law index, n, on the dimensionless skin friction coefficient $\left((1-n)\,\xi f''(\xi,0) + \frac{nW_e}{2}\xi\left(f''(\xi,0)\right)^2\right)$ and heat transfer rate $\left(\theta'(\xi,0)\right)$ at the sphere surface. The skin friction (Fig. 8a)

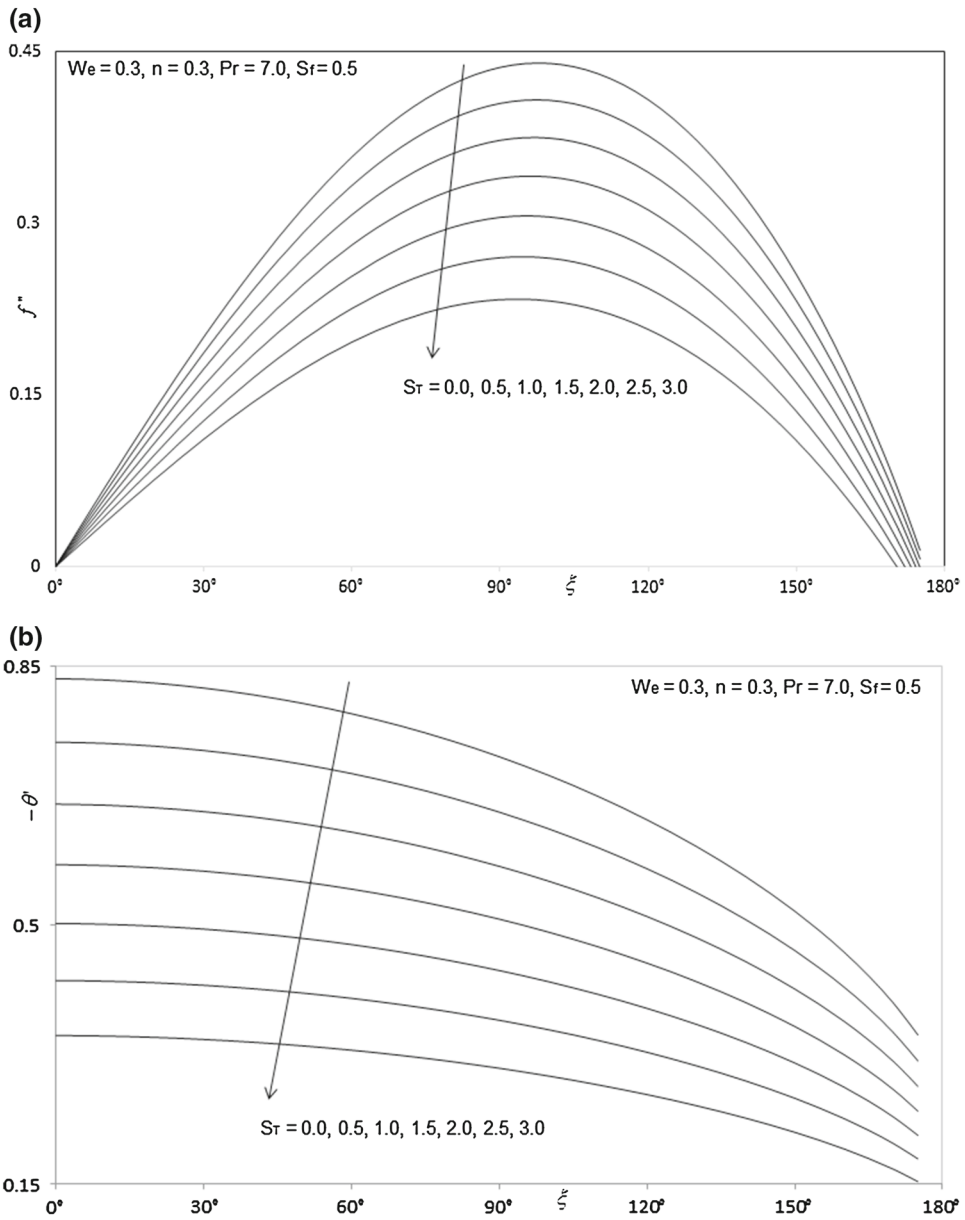

Fig. 10 **a** Influence of S_T on skin friction coefficient result. **b** Influence of S_T on Nusselt number result

at the sphere surface is reduced with increasing n,, however, only for very large values of the transverse coordinate, ξ. However, heat transfer rate (local Nusselt number) is enhanced with increasing n, again at large values of ξ, as computed in Fig. 8b.

Figure 9a, b presents the influence of the velocity slip, S_f, on the dimensionless skin friction coefficient $\left((1-n)\,\xi f''(\xi,0)+\frac{nW_e}{2}\xi\left(f''(\xi,0)\right)^2\right)$ and heat transfer rate $\left(\theta'(\xi,0)\right)$ at the sphere surface. With an increase in S_f, wall shear stress is consistently reduced. This trend was observed by Yazdi et al. [58] and Wang [59] using asymptotic methods. There is a progressive migration in the peak shear stress locations further from the lower stagnation point, as wall slip parameter is increased. With an increasing S_f, the local Nusselt number considerably increased.

Figure 10a, b presents the effect of thermal jump, S_T, on the dimensionless skin friction coefficient $\left((1-n)\,\xi f''(\xi,0)+\frac{nW_e}{2}\xi\left(f''(\xi,0)\right)^2\right)$ and heat transfer rate $\left(\theta'(\xi,0)\right)$ at the sphere surface. Increasing S_T is found to decrease both skin friction coefficient and local Nusselt number. For lower values of thermal jump, the plots are similar to those in Fig. 9b, and have a parabolic nature; however with S_T values greater than 1, the profiles lose their curvature and become increasingly *linear* in nature.

Table 5 Values of the local heat transfer coefficient $-\theta'(\xi, 0)$ for various values of ξ with $W_e = 0.0$, $n = 0.0$, $S_f = 0.0$, $S_T = 0.0$

ξ	$Pr = 0.7$					$Pr = 7.0$				
	Present	Nazar et al. [55]	% Difference	Molla et al. [56]	% Difference	Present	Nazar et al. [55]	% Difference	Molla et al. [56]	% Difference
0°	0.4572	0.4576	0.0437	0.4576	0.0437	0.9585	0.9595	0.0521	0.9582	0.0157
10°	0.4562	0.4565	0.0329	0.4564	0.0219	0.9560	0.9572	0.0627	0.9558	0.0105
20°	0.4534	0.4533	0.0110	0.4532	0.0220	0.9501	0.9506	0.0263	0.9492	0.0474
30°	0.4475	0.4480	0.0558	0.4479	0.0447	0.9390	0.9397	0.0373	0.9383	0.0373
40°	0.4402	0.4405	0.0341	0.4404	0.0227	0.9235	0.9239	0.0217	0.9231	0.0217
50°	0.4305	0.4308	0.0348	0.4307	0.0232	0.9042	0.9045	0.0166	0.9034	0.0443
60°	0.4186	0.4189	0.0358	0.4188	0.0239	0.8795	0.8801	0.0341	0.8791	0.0227
70°	0.4042	0.4046	0.0495	0.4045	0.0371	0.8505	0.8510	0.0294	0.8501	0.0235
80°	0.3872	0.3879	0.0903	0.3877	0.0645	0.8165	0.8168	0.0184	0.8161	0.0245
90°	0.3681	0.3684	0.0407	0.3683	0.0272	0.7772	0.7774	0.0129	0.7768	0.0257

6 Conclusions

Numerical solutions have been presented for the buoyancy-driven flow and heat transfer of tangent hyperbolic flow external to an isothermal sphere. The Keller-box implicit second order accurate finite difference numerical scheme has been utilized to efficiently solve the transformed, dimensionless velocity, and thermal boundary layer equations, subject to realistic boundary conditions. Excellent correlation with previous studies has been demonstrated testifying to the validity of the present code. The computations have shown that:

1. Increasing Weissenberg number, *We*, and the magnetic parameter, M, reduces the velocity, skin friction (surface shear stress), and heat transfer rate, whereas it elevates temperatures in the boundary layer.
2. Increasing power law index, n, increases the velocity and Nusselt number for all values of radial coordinate, i.e., throughout the boundary layer regime, whereas it depresses temperature and skin friction.
3. Increasing velocity slip, S_f, increases velocity and heat transfer rate but decreases temperature and skin friction (surface shear stress).
4. Increasing thermal jump, S_T, decreases velocity, temperature, skin friction and hear transfer rate.
5. Increasing transverse coordinate (ξ) generally decelerates the flow near the sphere surface and reduces momentum boundary layer thickness whereas it enhances temperature and therefore increases thermal boundary layer thickness in tangent hyperbolic non-Newtonian fluids.

Generally, very stable and accurate solutions are obtained with the present finite difference code. The numerical code is able to solve nonlinear boundary layer equations very efficiently and therefore shows excellent promise in simulating transport phenomena in other non-Newtonian fluids (Table 5).

References

1. Ramachandra Prasad, V.; Subba Rao, A.; Bhaskar Reddy, N.; Vasu, B.; Anwar Bég, O.: Modelling laminar transport phenomena in a Casson rheological fluid from a horizontal circular cylinder with partial slip. Proc. IMechE Part E J. Process Mech. Eng. (2013). doi:10.1177/0954408912466350
2. Norouzi, M.; Davoodi, M.; Anwar Bég, O.; Joneidi, A.A.: Analysis of the effect of normal stress differences on heat transfer in creeping viscoelastic Dean flow. Int. J. Therm. Sci. **69**, 61–69 (2013)
3. Uddin, M.J.; Yusoff, N.H.M.; Anwar Bég, O.; Ismail, A.I.: Lie group analysis and numerical solutions for F non-Newtonian nanofluid flow in a porous medium with internal heat generation. Physica Scripta **87**(14pp) (2013)
4. Rashidi, M.M.; Keimanesh, M.; Anwar Bég, O.; Hung, T.K.: Magneto-hydrodynamic biorheological transport phenomena in a porous medium: A simulation of magnetic blood flow control. Int. J. Numer. Meth. Biomed. Eng. **27**, 805–821 (2011)
5. Tripathi, D.; Pandey, S.K.; Anwar Bég, O.: Mathematical modelling of heat transfer effects on swallowing dynamics of viscoelastic food bolus through the human oesophagus. Int. J. Therm. Sci. **70**, 41–53 (2013)
6. Sparrow, E.M.; Lin, S.H.: Laminar heat transfer in tubes under slip-flow conditions. ASME J. Heat Transf. **84**, 363–639 (1962)
7. Inman, R.M.: Heat transfer for laminar slip flow of a rarefied gas in a parallel plate channel or a circular tube withuniform wall temperature. NASA Tech. Report, D-2213 (1964)
8. Larrode, F.E.; Housiadas, C.; Drossinos, Y.: Slip-flow heat transfer in circular tubes. Int. J. Heat Mass Transf. **43**, 2669–2680 (2000)
9. Spillane, S.: A study of boundary layer flow with no-slip and slip boundary conditions. PhD Thesis, Dublin Inst. of Technology, Ireland (2007)
10. Crane, L.J.; McVeigh, A.G.: Slip flow on a microcylinder. Z. Angew. Math. Phys. **61**(3), 579–582 (2010)

11. Ameel, T.A.; Barron, R.F.; Wang, X.M.; Warrington, R.O.: Laminar forced convection in a circular tube with constant heat flux and slip flow. MicroscaleThermophys. Eng. **1**, 303–320 (1997)
12. Yu, S.P.; Ameel, T.A.: Slip-flow convection in isoflux rectangular microchannel. ASME J. Heat Transf. **124**, 346–355 (2002)
13. Crane, L.J.; McVeigh, A.G.: Uniform slip flow on a cylinder. PAMM: Proc. Appl. Math. Mech. **10**, 477–478 (2010)
14. Anwar Bég, O.; Zueco, J.; Lopez-Ochoa, L.M.: Network numerical analysis of optically thick hydromagnetic slip flow from a porous spinning disk with radiation flux, variable thermophysical properties, and surface injection effects. Chem. Eng. Commun. **198**, 360–384 (2011)
15. Wang, C.Y.; Ng, C.-O.: Slip flow due to a stretching cylinder. Int. J. Non-Linear Mech. **46**, 1191–1194 (2011)
16. Lin, T.C.; Schaaf, S.A.: Effect of Slip on Flow Near a Stagnation Point and in a Boundary Layer. NACATN-2568 (1951)
17. Maslen, S.H.: Second Approximation to Laminar Compressible Boundary Layer on Flat Plate in Slip Flow. NACATN-2818 (1952)
18. Nonweiler, T.: The Laminar Boundary Layer in Slip Flow. College of Aeronautics Cranfield Univ., Rept. 62, Cranfield, England, U.K., (1952)
19. Reddy, K.C.: Thermal boundary layer in slip flow regime. AIAA J. **1**(10), 2396–2398 (1963). doi:10.2514/3.2078
20. Kogan, M.N.: Rare Fied Gas Dynamics. Plenum, New York (1969)
21. Hasimoto, H.: Boundary-layer slip solutions for a flat plate. J. Aeronaut. Sci. **25**(1), 68–69 (1958)
22. Pozzi, A.: Similar solutions in boundary layer slip flow. AIAA J. **1**(5), 1219–1219 (1963)
23. Wuest, W.: Boundary layers in rarefied gas flow. Prog. Aerosp. Sci. **8**, 295–352 (1967). doi:10.1016/0376-0421(67)90006-1
24. Maslen, S.H.: Second-order effects in laminar boundary layers. AIAA J. **1**(1), 33–40 (1963). doi:10.2514/3.1462
25. Van Dyke, M.: Higher order boundary layer theory. Annu. Rev. Fluid Mech. **1**, 265–292 (1969). doi:10.1146/annurev.fl.01.010169.001405
26. Gombosi, T.A.: Gaskinetic Theory. Cambridge Univ. Press, Cambridge (2002)
27. Ho, C.M.; Tai, Y.-C.: Micro-electro-mechanical-systems (MEMS) and fluid flows. Annu. Rev. Fluid Mech. **30**, 579–612 (1998). doi:10.1146/annurev.fluid.30.1.579
28. Gad-el-Hak, M.: The fluid mechanics of micro devices: the freeman scholar lecture. J. Fluids Eng. **121**(1), 5–33 (1999). doi:10.1115/1.2822013
29. Pop, I.; Ingham, D.B.: Convective heat transfer: mathematical and computational modelling of viscous fluids and porous media. Pergamon, Amsterdam (2001)
30. Nadeem, S.; Akram, S.: Peristaltic transport of a hyperbolic tangent fluid model in an asymmetric channel. ZNA **64a**, 559–567 (2009)
31. Nadeem, S.; Akram, S.: Magnetohydrodynamic peristaltic flow of a hyperbolic tangent fluid in a vertical asymmetric channel with heat transfer. Acta Mech. Sin. **27**(2), 237–250 (2011). doi:10.1007/s10409-011-0423-2
32. Akram, S.; Nadeem, S.: Simulation of heat and mass transfer on peristaltic flow of hyperbolic tangent fluid in an asymmetric channel. Int. J. Numer. Meth. Fluids. (2012). doi:10.1002/fld.2751
33. Akbar, N.S.; Nadeem, S.; Haq R.U.; Khan, Z.H.: Numerical solution of Magnetohydrodynamic boundary layer flow of tangent hyperbolic fluid towards a stretching sheet. Indian J. Phys. doi:10.1007/s12648-013-0339-8
34. Amato, W.S.; Chi, T.: Free convection heat transfer from isothermal spheres in water. Int. J. Heat Mass Transf. **15**, 327–339 (1972)
35. Liew, K.S.; Adelman, M.: Laminar natural heat transfer from an isothermal sphere to non-Newtonian fluids. Can. J. Chem. Eng. **53**, 494–499 (1975)
36. Amato, W.S.; Chi, T.: Free convection heat transfer from isothermal spheres in polymer solutions. Int. J. Heat Mass Transf. **19**, 1257–1266 (1976)
37. Churchill, S.W.: Comprehensive, theoretically based, correlating equations for free convection from isothermal spheres. Chem. Eng. Commun. **24**, 339–352 (1983)
38. Lien, F.-S.; Chen, C.-K.: Mixed convection of micropolar fluid about a sphere with blowing and suction. Int. J. Eng. Sci. **25**, 775–784 (1987)
39. Jia, H.; Gogos, G.: Laminar natural convection transfer from isothermal spheres. Int. J. Heat Mass Transf. **39**, 1603–1615 (1996)
40. Sharma, O.P.; Bhatnagar, R.K.: Low Reynolds number heat transfer from a sphere in a laminar flow of non-Newtonian fluids. uZAMM-Zeitschrift fr Angewandte Mathematik Und Mechanik **55**, 235–242 (1975)
41. Anwar Bég, O.; Zueco, J.; Bhargava, R.; Takhar, H.S.: Magnetohydrodynamic convection flow from a sphere to a non-Darcian porous medium with heat generation or absorption effects: network simulation. Int. J. Therm. Sci. **48**, 913–921 (2009)
42. Potter, J.N.; Riley, N.: Free convection from a heated sphere at large Grashof number. J. Fluid Mech. **100**, 769–783 (1980)
43. Prhashanna, A.; Chhabra, R.P.: Free convection in power-law fluids from a heated sphere. Chem. Eng. Sci. **65**, 6190–6205 (2010)
44. Chen, H.-T.; Chen, C.-K.: Natural convection of a non-Newtonian fluid about a horizontal cylinder and a sphere in a porous medium. Int. Comm. Heat Mass Transf. **15**, 605–614 (1988)
45. Dhole, S.D.; Chhabra, R.P.; Eswaran, V.: Forced convection heat transfer from a sphere to non-Newtonian power law fluids. AIChemE J. **52**, 3658–3667 (2006)
46. Anwar Bég, O.; Prasad, V.R.; Vasu, B.; Bhaskar Reddy, N.; Li, Q.; Bhargava, R.: Free convection heat and mass transfer from an isothermal sphere to a micropolar regime with Soret/Dufour effects. Int. J. Heat Mass Transf. **54**, 9–18 (2011)
47. Prasad, V.R.; Vasu, B.; Anwar Bég, O.; Parshad D., R.: Thermal radiation effects on magnetohydrodynamic free convection heat and mass transfer from a sphere in a variable porosity regime, Comm. Nonlinear Sci. Numer. Simul. **17**, 654–671 (2012)
48. Yih, K.A.: Viscous and Joule Heating effects on non-Darcy MHD natural convection flow over a permeable sphere in porous media with internal heat generation. Int. Commun. Heat Mass Transf. **27**(4), 591–600 (2000)
49. Keller, H.B.: Numerical methods in boundary-layer theory. Ann. Rev. Fluid Mech. **10**, 417–433 (1978)
50. Subhas Abel, M.; Datti, P.S.; Mahesha, N.: Flow and heat transfer in a power-law fluid over a stretching sheet with variable thermal conductivity and non-uniform heat source. Int. J. Heat Mass Transf. **52**, 2902–2913 (2009)
51. Chen, C.-H.: Magneto-hydrodynamic mixed convection of a power-law fluid past a stretching surface in the presence of thermal radiation and internal heat generation/absorption. Int. J. Non-Linear Mech. **44**, 596–603 (2009)
52. Zhang, Y.L.; Vairavamoorthy, K.: Analysis of transient flow in pipelines with fluid-structure interaction using method of lines. Int. J. Numer. Meth. Eng **63**, 1446–1460 (2005)
53. Kumari, M.; Nath, G.: Steady mixed convection stagnation-point flow of upper convected Maxwell fluids with magnetic field. Int. J. Nonlinear Mech. **44**, 1048–1055 (2009)
54. Cebeci, T.; Bradshaw, P.: Momentum Transfer in Boundary Layers. Hemisphere, Washington (1977)
55. Nazar, R.; Amin, N.; Grosan, T.; Pop, I.: Free convection boundary layer on an isothermal sphere in a micropolar fluid. Int. Comm. Heat Mass Transf. **29**(3), 377–386 (2002)
56. Molla, Md.M.; Taher, M.A.; Chowdhury, Md.M.K.; Hossain, Md.A.: Magnetohydrodynamic natural convection flow on a sphere in presence of heat generation. Nonlinear Anal. Model. Control **10**(4), 349–363 (2005)

57. Ajadi, S.O.; Adegoke, A.; Aziz, A.: Slip boundary layer flow of non-Newtonian fluid over a flat plate with convective thermal boundary condition. Int. J. Nonlinear Sci. **8**, 300–306 (2009)
58. Yazdi, M.H.; Abdullah, S.; Hashim, I.; Sopian, K.: Slip MHD liquid flow and heat transfer over non-linear permeable stretching surface with chemical reaction. Int. J. Heat Mass Transf. **54**, 3214–3225 (2011)
59. Wang, C.Y.: Stagnation flow on a cylinder with partial slip–an exact solution of the Navier-Stokes equations. IMA J. Appl. Math. **72**, 271–277 (2007)